Experiments on a Model Helicopter Rotor Operating in the Vortex Ring State

KYUICHIRO WASHIZU* AND AKIRA AZUMA†
University of Tokyo, Tokyo, Japan

AND

JIRO KŌO‡ AND TŌICHI OKA‡
National Aerospace Laboratory, Tokyo, Japan

Unsteady aerodynamic characteristics of a model helicopter rotor operating in the vortex ring state have been experimentally investigated. Time histories of thrust, torque, and rpm of the rotor were measured by use of sensing devices that were installed on the shaft of the rotor. The results obtained show that in the vortex ring state, the thrust fluctuates violently, whereas the torque fluctuates very little; in fact, it is hardly observable. The induced power obtained from thrust and torque data has been compared with that obtained from the momentum theory. Existence of periodicity in the thrust fluctuation also has been observed in some regions of the vortex ring state.

Nomenclature

C_Q = $Q/\rho\pi R^5\Omega^2$ torque coefficient
C_{Q0} = profile torque coefficient
C_T = $T/\rho\pi R^4\Omega^2$ thrust coefficient
P_i = induced power
Q = torque
R = radius of the rotor
R/D = $V \sin\alpha$ rate of descent
T = thrust
V = flight velocity of the rotor
$\mathcal{V}$ = mean induced velocity based on the momentum theory and given by Eq. (9)
$\mathcal{V}_h$ = mean induced velocity at hover
$\bar{\mathcal{V}}$ = reference velocity defined by Eq. (5)
$\mathcal{V}_e$ = equivalent induced velocity based on the power consideration and given by Eq. (7)
α = angle between the rotor plane and the direction of flight of the rotor; the condition $\alpha = 90°$ corresponds to vertical descent
λ = $(C_T/2)^{1/2}$
θ = pitch angle of the blade
$\theta_{0.75}$ = pitch angle of the blade measured at 0.75 R
Ω = angular velocity of the rotor

Introduction

THE aerodynamic characteristics of a helicopter rotor operating in the vortex ring state has been of greatest concern in helicopter engineering. The importance of this problem has been emphasized recently by the Federal Aviation Agency (FAA) certification program for commercial helicopter operation involving aircraft recovery maneuvers in the event of single engine failure during vertical takeoff and landing. Although a number of papers have been written on this subject,[1-9] there still remain many questions to be answered. The purpose of the experiment described herein is to measure the unsteady aerodynamic characteristics of a single rotor operating in the vortex ring state.

A model basin was used for the quantitative measurement of the aerodynamic characteristics of the rotor. The rotor system was installed on a carriage that moves on the track of the model basin. The speed of the carriage V, the pitch angle of the blade θ, and the angle of attack of the rotor plane α were prescribed as variable parameters during the tests.

Early in 1959, the authors began their first studies on a rotor operating in the vortex ring state by conducting a series of experiments in a wind tunnel. It was soon found that as far as qualitative measurements of rotor characteristics are concerned, the wind tunnel provided a powerful tool; however, for quantitative measurements, the wind tunnel was not always reliable for several reasons. First, the wind tunnel had interference effects from the wall because of the size of the fluctuating air bubble or the so-called airbody around the rotor which extends to a distance of several rotor diameters in some conditions of the vortex ring state[6]; thus, the wind tunnel must be considerably larger than the diameter of the rotor being tested for good quantitative measurements. Second, it was difficult to find an existing wind tunnel having excellent low speed characteristics. Most of the available wind tunnels were designed so as to assure an optimum flow distribution at speeds around 25 ~ 50 m/sec. As a result, these wind tunnels usually have very poor characteristics in the speed range required for testing rotors in the vortex ring state. Third, the rotor induces a flowfield in the main stream of the wind tunnel. The aero-

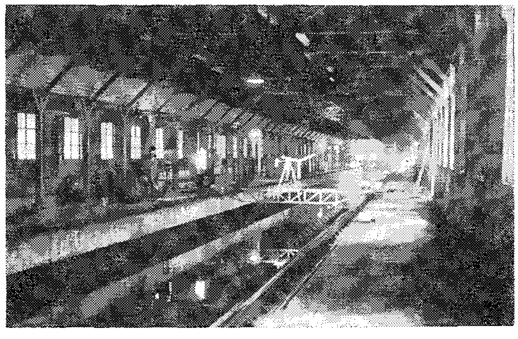

Fig. 1 Carriage.

Presented at the AIAA Symposium on Structural Dynamics and Aeroelasticity, Boston, Mass., August 30–September 1, 1965 (no preprint number; published in bound volume of preprints of the meeting); submitted October 19, 1965; revision received March 9, 1966.

* Professor of Aeronautics, Department of Aeronautics, Faculty of Engineering. Member AIAA.

† Associate Professor, Institute of Space and Aeronautical Science. Member AIAA.

‡ Research Engineer, Flight Research Division.

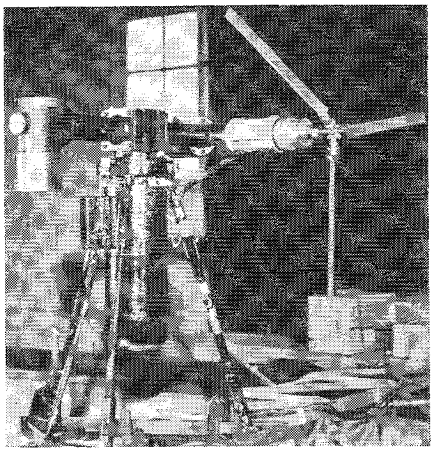

Fig. 2 Rotor assembly.

dynamic characteristics of the rotor flying in still air are needed. Such differences could be compensated for except that it is very difficult to find in the wind tunnel a satisfactory location for measuring flow speed that will correspond to the speed of the rotor flying in still air. Because of the foregoing reasons, the authors found that the use of the test track, on which a carriage loaded with the rotor system could move in still air, was indispensable for their experiments. A special carriage was designed which would operate in the speed range of $0 \sim 12$ m/sec. This carriage proved to be a very useful and powerful tool for experiments in low speed aerodynamics.

Test Apparatus

Model Basin and Carriage

As mentioned previously, the authors used a model basin for the rotor test. The main dimensions of the basin are as follows: the effective length of the track was 200 m, the width of the track was 5 m, the inner width of the building was 12 m, and the height of the ceiling from the floor was 4.7 m.

The rotor system, together with the measuring instruments and recorders, was installed on a carriage that was towed by a cable. One of the rolling wheels of the carriage triggered a photo-transistor that produced pulses to measure the carriage speed. The carriage is shown in Fig. 1.

Rotor Assembly

The blades of the rotor are made of duralumin and weigh 109 g a piece. The airfoil of each blade is a NACA 0012 section. The geometrical properties of the rotor are as follows: the diameter is 1 100 mm, the chord is 33 mm, the twist from root to tip is 8° 20′, the position of the flapping

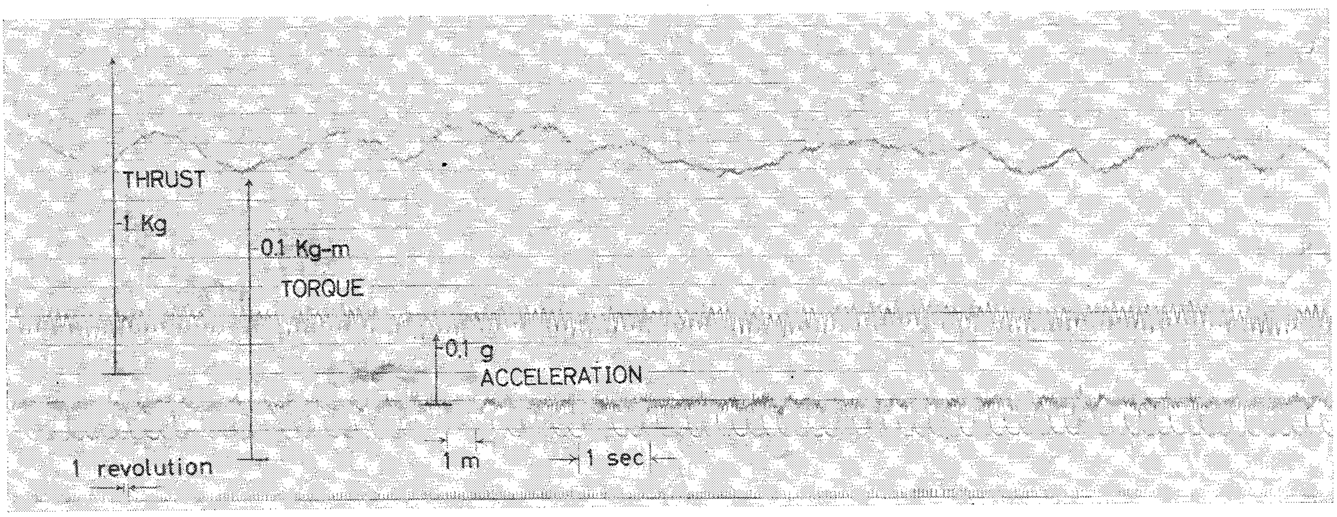

Fig. 3a Time histories of the thrust, torque, and rpm of the rotor; $V = 2.3$ m/sec, $\alpha = 90°$.

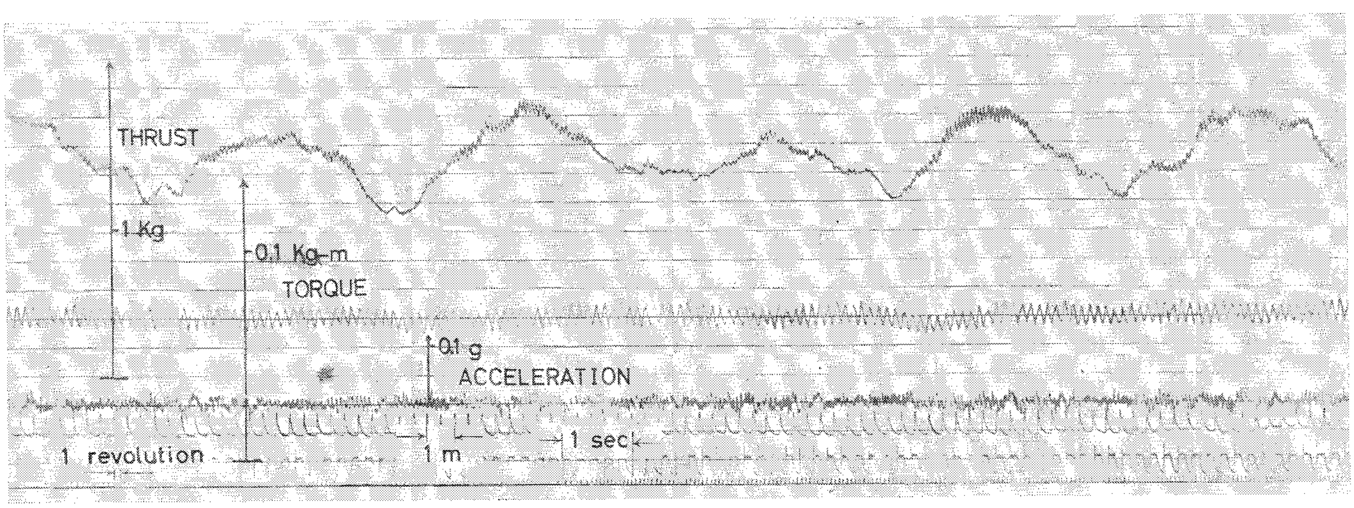

Fig. 3b Time histories of the thrust, torque, and rpm of the rotor; $V = 2.6$ m/sec, $\alpha = 60°$.

hinge is 0.0327 R, the position of the lagging hinge is 0.0327 R, the number of blades is three, and the solidity is 0.0573.

Each blade rotates around its 18% chord axis to set the pitch angle. The rotor can flap and lag. However, no cyclic pitch mechanism is employed. The rotor is driven by an 800-w d.c. motor through gear transmission at approximately 1000 rpm. The rotor assembly is shown in Fig. 2.

Instrumentation

The torque and thrust of the rotor are measured with strain gages. The torque pickup, which consists of a torsion tube and four strain gages, has a maximum capacity of 0.5 m-kg. The thrust pickup, which consists of four leaf springs and eight strain gages, has a maximum capacity of 5 kg. The outputs of these two pickups are delivered to the recording instruments through a slip ring assembly located on the rotor shaft beneath the pickups. The rate of revolution of the rotor is measured with pulses, which a small plate attached on the shaft produced by interrupting a light beam every revolution. These outputs finally are delivered to the recording instruments on the carriage.

It is noted here that a low pass filter was inserted between the measuring pickups and the recorders to reduce the effects of high frequency noise produced by mechanical vibrations of the rotor and running carriage. The characteristics of this filter were examined by use of a step response produced by a calibrating signal imposed on the thrust and torque measuring systems. It was found by representing this filter by a first-order linear system that its characteristic time was approximately 0.07 sec.

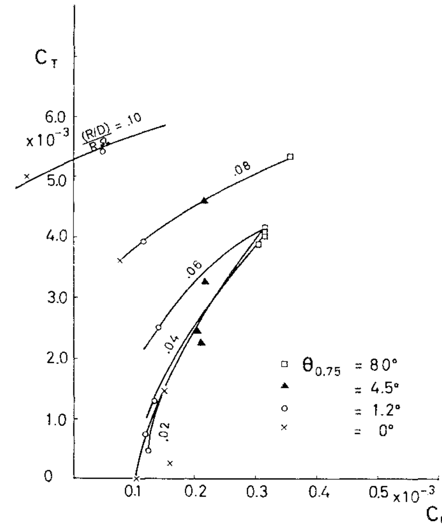

Fig. 5 **Thrust vs torque in polar curves.**

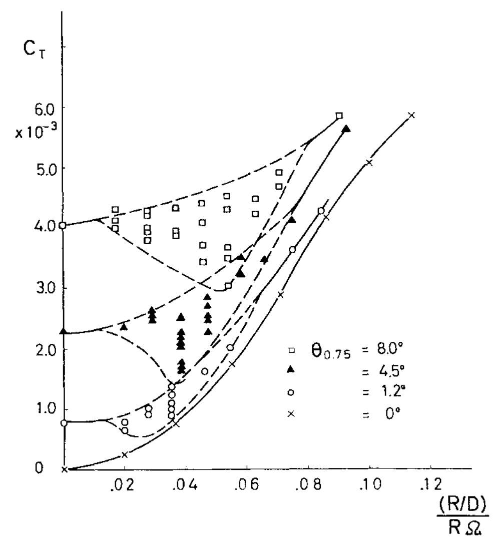

Fig. 4a **Thrust vs rate of descent.**

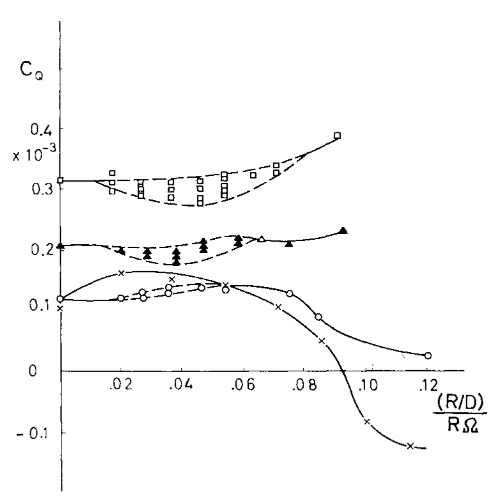

Fig. 4b **Torque vs rate of descent.**

Experimental Results

Typical Test Records

Time histories of the thrust, torque, and rpm of the rotor as well as the speed of the carriage were measured and recorded. Figures 3a and 3b show two typical test records for vertical and oblique descents, respectively. The presence of severe fluctuations of thrust are observed in these figures. It also is observed in Fig. 3b that there exists a marked periodicity in the thrust fluctuation.

Terms C_T and C_Q in Vertical Descent

The characteristics of C_T and C_Q of the rotor in vertical descent are shown in Figs. 4a and 4b, respectively, where the nondimensionalized vertical descent velocity $(R/D)/R\Omega$ is used as abscissa, and the blade pitch angle at 0.75 R is used as a variable parameter. In evaluating the points shown in these figures instantaneous values of thrust, torque, and rpm were taken directly from the test records and nondimensionalized. The mean values of C_T and C_Q are plotted in the form of polar curves in Fig. 5 using rate of descent as a variable parameter. It is observed in these figures that the rotor enters an autorotative state at high rates of descent when the pitch angle is small.

Induced Power

By using values of C_T and C_Q for hovering under the assumption of constant induced velocity over the rotor disk, one can calculate the profile torque coefficient C_{Q0} by the relation

$$C_{Q_0} = C_Q - C_{T_h}\lambda_h \tag{1}$$

where

$$C_{T_h} = T_h/\rho\pi R^4\Omega^2 \tag{2}$$

$$\lambda_h = (C_{T_h}/2)^{1/2} \tag{3}$$

and where the subscript h indicates that the quantity is related to hover. The profile torque coefficient will be treated in the following analysis as a function of C_T only, regardless of the rate of descent and angle of attack.

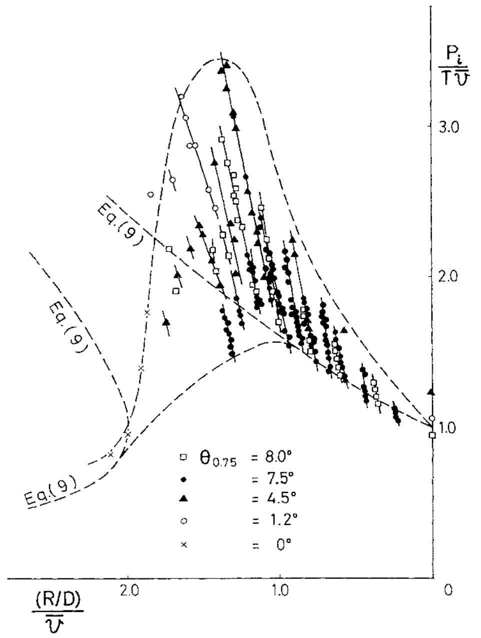

Fig. 6a Induced power vs rate of descent, $\alpha = 90°$.

With a further assumption that the component of the rotor force in the rotor plane is negligibly small, one can calculate the induced power P_i and a reference velocity $\bar{\mathcal{V}}$ as follows:

$$P_i = \rho\pi R^5\Omega^3(C_Q - C_{Q_0}) + (R/D)T \tag{4}$$

$$\bar{\mathcal{V}} = (T/2\rho\pi R^2)^{1/2} = R\Omega(C_T/2)^{1/2} \tag{5}$$

where R/D is the component of the rotor velocity in the shaft direction equal to $V \sin\alpha$. The induced power is related to the equivalent induced velocity $\mathcal{V}_e$, based on the power consideration, as follows:

$$P_i = T\mathcal{V}_e \tag{6}$$

Consequently, one obtains

$$\mathcal{V}_e = R\Omega\left[\frac{C_Q - C_{Q_0}}{C_T} + \frac{R/D}{R\Omega}\right] \tag{7}$$

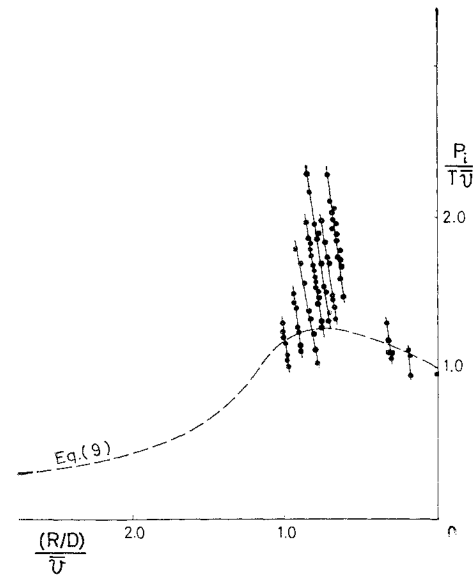

Fig. 6c Induced power vs rate of descent, $\alpha = 50°$.

Thus, one can define the induced power in nondimensiona form by the relation

$$P_i/T\bar{\mathcal{V}} = \mathcal{V}_e/\bar{\mathcal{V}} \tag{8}$$

It is noted here for later convenience that, if the momentum theory is assumed to be applicable even in the vortex ring state, one can calculate the mean induced velocity $\mathcal{V}$, based on the momentum consideration, using the following equation:

$$\frac{R/D}{\bar{\mathcal{V}}} = \frac{\mathcal{V}}{\bar{\mathcal{V}}}\sin^2\alpha \pm \sin\alpha\left[\left(\frac{\bar{\mathcal{V}}}{\mathcal{V}}\right)^2 - \left(\frac{\mathcal{V}}{\bar{\mathcal{V}}}\right)^2\cos^2\alpha\right]^{1/2} \tag{9}$$

The relation between the nondimensionalized induced power and rate of descent, i.e., $P_i/T\bar{\mathcal{V}}$ vs $(R/D)/\bar{\mathcal{V}}$, together with the relation between nondimensionalized mean induced velocity and rate of descent, i.e., $\mathcal{V}/\bar{\mathcal{V}}$ vs $(R/D)/\bar{\mathcal{V}}$, is plotted for $\alpha = 90°$, $70°$, $50°$, and $20°$ in Figs. 6a–6d, respectively. Points on these plots are obtained as follows. Read values

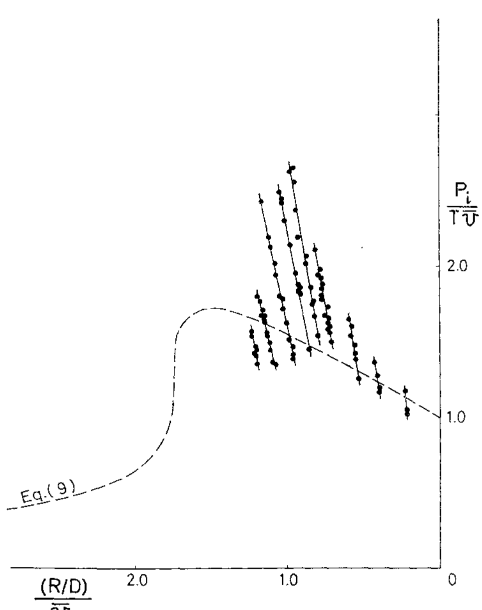

Fig. 6b Induced power vs rate of descent, $\alpha = 70°$.

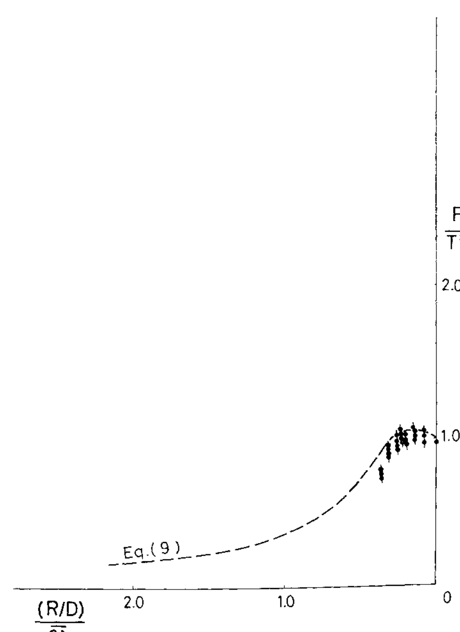

Fig. 6d Induced power vs rate of descent, $\alpha = 20°$.

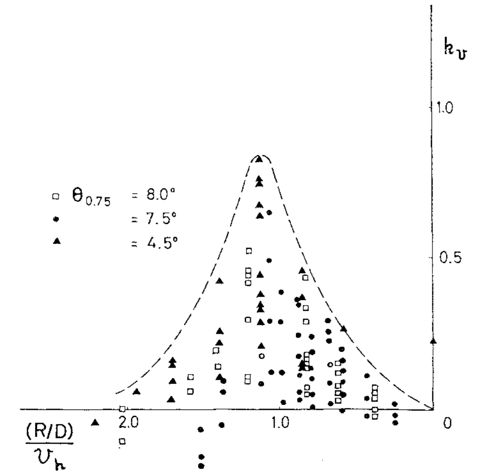

Fig. 7 Power loss factor vs rate of descent.

of the fluctuating thrust at its peaks and valleys from experimental records and read at the same times corresponding values of the torque and rates of revolution of the rotor. Then, values of $P_i/T\mathcal{V}$ can be calculated using Eq. (8).

It is observed from Figs. 6a–6c that a family of values of $[P_i/T\mathcal{V}, (R/D)/\mathcal{V}]$ obtained from a series of tests under a constant pitch angle and a constant rate of descent seems to lie on a single curve. Let the region covered by these lines be called "*TF* region"; thus emphasizing the region where thrust fluctuation is pronounced. It is interesting to observe that the lower boundary of the *TF* region seems to coincide with the curve given by the momentum theory except for those rates of descent where the vortex ring state seems most pronounced. The upper boundary of the *T-F* region may be determined by the characteristics of the fluctuating air bubble or by the growth and disappearance of the vortex ring around the rotor. In reading these figures, remember that since the speed of the carriage and the length of the track are limited, the accuracy of test results obtained at high pitch angles and high rates of descent may not be good. However, it may be observed from Fig. 6a that the flow pattern around the rotor in vertical descent begins to vary from the vortex ring state to the windmill brake state around $(R/D)/\mathcal{V} \approx 2$.

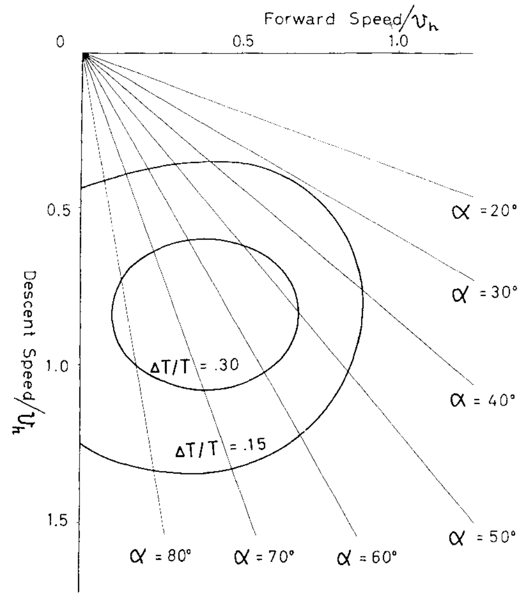

Fig. 8 $\Delta T/T$.

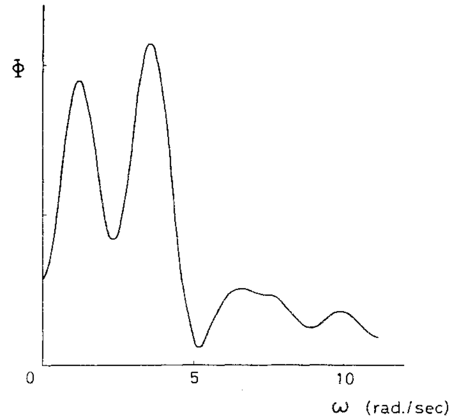

Fig. 9 An example of power spectral analysis; V = 4.1 m/sec, α = 60°.

It is considered convenient to introduce here a power loss parameter k_v defined by the relation

$$k_v = (\mathcal{V}_e/\mathcal{V}) - 1 \tag{10}$$

Using this parameter, one can calculate increments of the equivalent induced velocity compared to the mean induced velocity obtained from the momentum theory. It may be said that the power loss factor is a measure of the induced power wastefully fed to the air flow around the rotor. Values of k_v for the rotor in vertical descent are plotted in Fig. 7, where $\mathcal{V}$ is calculated from Eq. (9) by setting α = 90° and employing the negative sign.

Thrust Fluctuation

Another way of representing the region where the vortex ring state occurs may be to use $\Delta T/T$, where ΔT and T are the amplitude of fluctuation and mean value of the thrust, respectively. These values are taken from the records and plotted in Fig. 8 with the value of $\Delta T/T$ as a variable parameter. It is noted that this figure was obtained using a limited number of the experimental results and therefore should be considered only as an indication of the $\Delta T/T$ characteristics in the vortex ring state. More experimental data and statistical procedures are considered indispensable for a definite determination of the contours.

Periodicity of the Thrust Fluctuation

As shown in Fig. 3b, a marked periodicity exists in the thrust fluctuation in some regions of the vortex ring state.

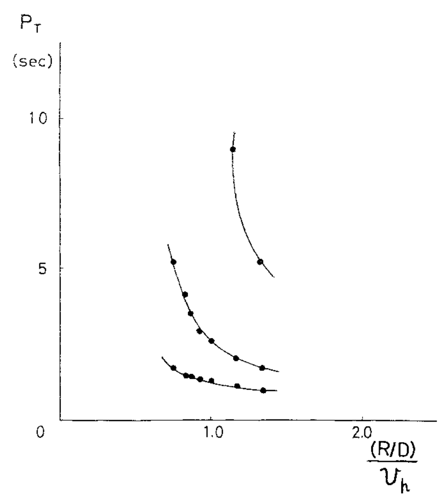

Fig. 10 Period vs rate of descent, α = 60°.

For the purpose of finding periodicity, the power spectral density method was applied. An example of the power spectral analysis is shown in Fig. 9. From figures such as this, periods of the thrust fluctuation with dominant power are obtained for the rotor in a oblique descent and plotted in Fig. 10 with rate of descent used as abscissa. These figures show that in some region of the vortex ring state there exists a fairly pronounced periodicity that has a structure similar to those observed in the wake of a circular disk or cylinder.

Conclusions

Some of the quantitative characteristics of the flow around a single model rotor operating in the vortex ring state have been obtained from the experiments conducted at the model basin. However, further experiments should be conducted on model as well as full-scale rotors before the results presented herein can be proved applicable to the operation of a helicopter. It should be added that the fuselage as well as the tail rotor may have significant effects on the aerodynamics as well as the stability and control of a helicopter operating in the vortex ring state.

References

[1] Glauert, H., "The analysis of experimental results in the windmill brake and vortex ring states of an airscrew," Aeronautical Research Committee, Rept. and Memo. 1026 (1926).

[2] Lock, C. N. H., "Note on the characteristic curve of an airscrew of helicopter," Ministry of Supply, Aeronautical Research Council, Rept. and Memo. 2673 (1952).

[3] Brotherhood, P., "Flow through a helicopter rotor in vertical descent," Ministry of Supply, Aeronautical Research Council, Rept. and Memo. 2735 (1952).

[4] Stewart, W., "Helicopter behavior in the vortex ring conditions," Ministry of Supply, Aeronautical Research Council, Rept. and Memo. 3117 (1959).

[5] Castles, W., Jr. and Gray, R. B., "Experimental relation between induced velocity, thrust and rate of descent of a helicopter rotor as determined by windtunnel tests on four model rotors," NACA TN 2474 (1951).

[6] Meijer Drees, J. and Hendal, W. P., "Airflow patterns in the neighborhood of helicopter rotors," Aircraft Eng. **23**, 107–111 (1951).

[7] Gessow, A. and Myers, G. C., Jr., *Aerodynamics of the Helicopter* (The MacMillan Co., New York, 1952).

[8] Stepniewski, W. Z., *Introduction to Helicopter Aerodynamics* (Edwards Brothers Inc., Ann Arbor, Mich., 1958).

[9] Castles, W., Jr., "Flow induced by a rotor in power-on vertical descent," NACA TN 4330 (1958).